高结晶度氮掺杂介孔 TiO₂ 的制备及光催化活性

刘二强[1], 郭晓玲[2], 秦　雷[1], 申国栋[2], 王向东[1,*]

[1]西安交通大学理学院, 陕西西安 710049

[2]西安工程大学纺织与材料学院, 陕西西安 710048

摘要: 以钛酸丁酯为钛源, 尿素为氮源, 聚丙烯酰胺 (PAM) 和聚乙二醇 (PEG) 为复合模板剂, 采用溶胶-凝胶法, 在氮气和空气气氛中分段煅烧, 制得高结晶度氮掺杂介孔 TiO₂ 光催化剂. 利用 X 射线衍射、透射电镜、N₂ 吸附-脱附、X 射线光电子能谱和紫外-可见漫反射光谱等技术对其进行了表征. 结果表明, 当 PAM 和 PEG 的质量比为 1:4 时, 先在氮气中 600 °C 煅烧, 后在空气中 500 °C 煅烧所得样品是锐钛矿相, 具有良好的孔隙结构和较高的结晶度, 平均孔径为 5.11 nm, 晶粒尺寸为 12.5 nm, 比表面积 110.8 m²/g. 掺杂介孔 TiO₂ 的氮主要以取代氮和化学吸附分子 γ-N₂ 的形式存在, 少量以间隙氮形式存在. 氮掺杂使 TiO₂ 的能带变窄, 吸收带边明显红移, 且使光吸收强度显著增大. 光催化降解甲基橙实验结果表明, 与未掺杂样品相比, 氮掺杂介孔 TiO₂ 在可见光作用下表现出较高的催化活性.

关键词: 介孔二氧化钛; 氮掺杂; 高结晶度; 光催化活性; 甲基橙

中图分类号: O643   **文献标识码**: A

Fabrication and Photocatalytic Activity of Highly Crystalline Nitrogen Doped Mesoporous TiO₂

LIU Erqiang[1], GUO Xiaoling[2], QIN Lei[1], SHEN Guodong[2], WANG Xiangdong[1,*]

[1]*School of Science, Xi'an Jiaotong University, Xi'an 710049, Shaanxi, China*

[2]*School of Textile and Materials, Xi'an Polytechnic University, Xi'an 710048, Shaanxi, China*

Abstract: Highly crystalline nitrogen doped mesoporous TiO₂ photocatalysts were fabricated by the sol-gel method using tetrabutyl titanate as the Ti source, urea as the N source, and polyacrylamide (PAM) and polyethylene glycol (PEG) as the templates, and then by calcining in nitrogen and air. The photocatalysts were characterized by X-ray diffraction, transmission electron microscopy, N₂ adsorption, X-ray photoelectron spectroscopy, and UV-Vis spectroscopy. When the mass ratio of PAM and PEG was 1:4, the sample prepared by calcining at 600 °C in nitrogen and 500 °C in air had the anatase phase and a mesoporous structure and high crystallinity. The average pore size, crystallite size, and specific surface area were 5.11 nm, 12.5 nm, and 110.8 m²/g, respectively. Nitrogen atoms were incorporated into the TiO₂ lattice mainly as substitutional N and molecularly chemisorbed γ-N₂, and a small amount of interstitial N. Nitrogen doping narrowed the band gap and allowed light absorption in the visible light region. Compared with undoped mesoporous TiO₂, the absorption band edge of nitrogen doped samples exhibited a red shift and the light absorption intensity was increased. Photocatalytic degradation of methyl orange showed that the nitrogen doped mesoporous TiO₂ had a higher photocatalytic activity than undoped mesoporous TiO₂ under visible light.

Key words: mesoporous titanium dioxide; nitrogen doped; high crystallinity; photocatalytic activity; methyl orange

Mesoporous TiO_2 is well studied because of its photocatalytic activity, which is used in photoelectrochemical applications [1−7]. Mesoporous TiO_2 prepared by traditional methods still has some disadvantages such as low crystallinity, low thermostability, and low visible light response. Mesoporous TiO_2 with enhanced crystallinity and thermostability is required in many demanding applications, such as solar energy conversion, batteries, and photocatalysis, because the semiconducting and photovoltaic behavior is largely dependent on the crystallinity of the TiO_2. Many approaches have been taken to improve the crystallinity of mesoporous TiO_2, including using several block copolymers as templates to give a much thicker pore wall composed of nanocrystals embedded in an amorphous material [8−10]. When these materials are converted into the completely crystalline state at high temperature, the mesoporous structure collapses due to the growth of the nanocrystals. Despite much effort, it is a major challenge to successfully convert the amorphous walls of mesoporous TiO_2 to crystalline walls while retaining the original mesoporous structure.

To solve the above problem, Lee et al. [11] reported a new method in which an amphiphilic diblock copolymer, poly(isoprene-block-ethylene oxide), was used as the template to synthesize mesoporous TiO_2, which was then calcined in an Ar atmosphere first and then recalcined in air. The mesoporous TiO_2 prepared by this method has high crystallinity, high thermostability, and high surface area. However, the disadvantage of the method is the cost of the template. Their study did not report about TiO_2 doping especially with nonmetal elements such as N [12−15], F [16,17], S [18], and C [19,20], which can create a mid-gap state that acts as electron donor or acceptor in the band gap of TiO_2. The doping can narrow the band gap of TiO_2 and extend its light absorption into the visible region, which would then enhance the quantum efficiency of the material, improving its photocatalytic activity under visible light.

In the present paper, we report a sol-gel method using polyacrylamide (PAM) and polyethylene glycol (PEG) as templates to synthesis nitrogen doped mesoporous TiO_2 with high surface area and high crystallinity. The materials were characterized by X-ray diffraction (XRD), transmission electron microscopy (TEM), N_2 adsorption, X-ray photoelectron spectroscopy, and UV-Vis spectroscopy. The photocatalytic activities of the undoped and nitrogen doped mesoporous TiO_2 were evaluated by the photocatalytic degradation of methyl orange (MO) in water.

1 Experimental

1.1 Photocatalyst synthesis

The sol-gel preparation of the nitrogen doped mesoporous TiO_2 was performed as follows. Deionized water (10 ml), nitric acid (5 wt%, 6 ml), and 0.5−6.0 g of urea dissolved in 280 ml of absolute ethanol were added into 10 ml of tetrabutyl titanate. After the mixture was stirred at ambient temperature for 1 h, the resulting solution was slowly added into a solution of 0.2 g PAM (Wt = 3000000) and 0.8 g PEG (Wt = 20000) dissolved in 30 ml of deionized water under vigorously stirring. A white gel was formed, which was dried at 60 °C for 12 h. The light yellow powder obtained was calcined in a N_2 atmosphere and 400−800 °C, and then recalcined in air at 400−700 °C. For comparison, undoped mesoporous TiO_2 was prepared according to the above procedure with the absence of urea.

1.2 Photocatalyst characterization

XRD patterns of the photocatalysts were recorded at room temperature by a Bruker D8 Advance X-ray diffractometer using Cu K_α radiation and a scan rate of 2°/min. TEM image was recorded on a JEM-2100F made in Japan. N_2 adsorption isotherms were collected on an AUTOSORB-1 nitrogen adsorption apparatus at −196 °C. XPS analysis was performed using a PHI 5300 ESCA instrument with an Mg K_α X-ray source at a power of 250 W. The binding energy was calibrated with respect to the C $1s$ peak of hydrocarbon contamination at 284.6 eV. Diffuse reflectance UV-visible absorption spectra of the powder samples were obtained using a Shimadzu-2501 spectrophotometer. $BaSO_4$ was the reference sample, and the spectra were recorded in the range of 200−900 nm.

1.3 Photocatalytic activity

Photocatalytic activity was tested by the photocatalytic degradation of MO solutions under visible light irradiation at room temperature. The reactor was a 100 ml cylindrical vessel containing 60 ml of MO solution with a water-cooled quartz jacket. Irradiation was by a 300 W xenon lamp located in the center of the quartz jacket, which emitted a similar spectrum to visible light. This was equipped with a magnetic stirrer at the bottom of the reactor to achieve effective dispersion. The initial MO concentration was 10 mg/L and the amount of photocatalyst was 150 mg. Before irradiation, 30 min adsorption was allowed to reach adsorption equilibrium with the photocatalyst and MO solutions were kept in a dark condition. Then the mixed solution was irradiated. The solution (4 ml) was taken out at regular intervals and separated by centrifugal separation to determine the residual concentration of MO by a spectrophotometer (UV-7220, Beifenruili, China) at 464 nm. The change of relative absorbance was used to record the change of concentration of MO in the solution.

2 Results and discussion

2.1 Photocatalyst synthesis

Figure 1 shows the synthesis mechanism of the photocatalysts. The nitrogen doped mesoporous TiO_2 was prepared by two steps. First, a sol-gel process was conducted using tetrabutyl titanate as the Ti source, urea as the N source, and PAM and PEG as the templates. Due to its strong hydrophilicity, PEG readily combined with the titania sol obtained from the hydrolyzation to form composite grains. These composite grains were incorporated in PAM by hydrogen bonding, and the grains were confined in the molecule network of PAM. This bonding process can effectively accelerate the sol-gel reaction. Second, the precursor prepared by the sol-gel process was successively calcined in a N_2 atmosphere and air atmosphere to synthesize the photocatalyst. Nitrogen doped mesoporous TiO_2 with a high crystallinity and high surface area was obtained. This was because in this method, PEG was easily decomposed on heating, whereas the more thermally stable PAM was converted to a sturdy, amorphous carbon when calcined in N_2. The amorphous carbon acted as a rigid support of the mesoporous structure that prevented its collapse when it was calcined to the temperature required for getting a highly crystalline material [11]. The carbon was subsequently eliminated by calcining in air, leaving a highly crystalline mesoporous material.
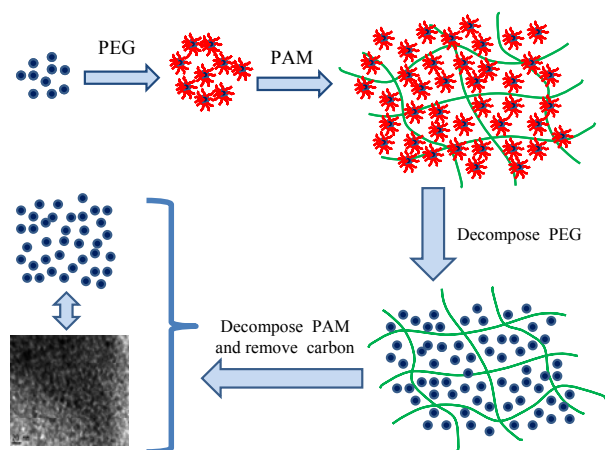

Fig. 1. Illustration of the synthesis mechanism of the photocatalysts.

2.2 XRD analysis

Figure 2 shows the XRD patterns of the nitrogen doped mesoporous TiO_2 prepared with the PAM:PEG mass ratio 1:4 after calcination at different temperatures. The phase composition of the samples was mainly anatase and an amorphous phase when the calcining temperature was low (Figs. 2(1) and (2)). The rutile phase appeared when the
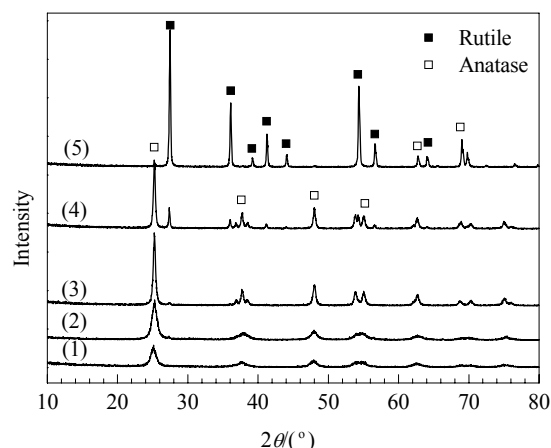

Fig. 2. XRD patterns of samples calcined at different temperatures (N_2/air). (1) 400/400 °C; (2) 500/400 °C; (3) 600/500 °C; (4) 700/600 °C; (5) 800/700 °C.

calcining temperature was 700/600 °C (Fig. 2(4)), and it was the main phase when the temperature was 800/700 °C (Fig. 2(5)). It was a good calcining temperature (600/500 °C, Fig. 2(3)) because the phase composition of the sample was mainly anatase and it has a high specific surface areas (Table 1). The diffraction peak became significantly sharper with the increase in calcining temperature, indicating an increase in crystallinity [13,21]. The average crystallite size of the anatase crystals, estimated from the X-ray peak width using the Scherrer equation, became larger with the increase of the calcining temperature (Table 1). The specific surface area decreased sharply with the increase in calcining temperature. So, in this method, the calcining temperature of 600 (in N_2) and 500 °C (in air) were appropriate to optimize the crystallinity, crystal phase, and specific surface area.

Table 1 Characterization results of samples prepared at different temperatures

T/°C		A_{BET}/	Phase	Crystallite size
N_2	air	m²/g		(nm)
400	400	171.2	A + Amors.	9.45
500	400	135.2	A + Amors.	9.36
600	500	110.8	A	12.46
700	600	42.3	A	21.35
800	700	19.8	A + R	25.47 + 41.38

A: anatase phase; R: rutile phase; Amors: amorphous phase.

2.3 TEM analysis

Figure 3 shows the TEM images of the sample prepared at the calcination temperature of 600/500 °C. It can be seen from Fig. 3(a) that the sample has a typical honeycomb porous structure with high crystallinity, in which the agglomeration of monodispersed TiO_2 particles was clearly ob-
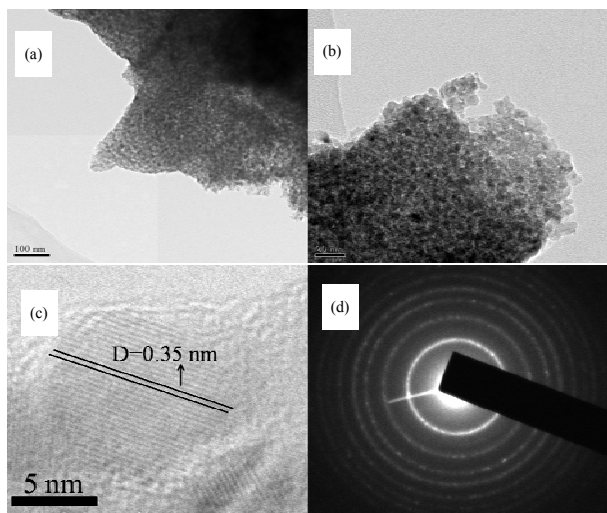
Fig. 3. Samples characterized by TEM. (a,b) TEM images; (c) HRTEM image; (d) SAED pattern.

served. Figure 3(b) shows that the sample has a wormhole-like pore structure. The pores were connected randomly and lack a discernible long range order in the pore arrangement. Anatase TiO_2 nanocrystals were embedded in the disordered mesoporous framework. As seen in Fig.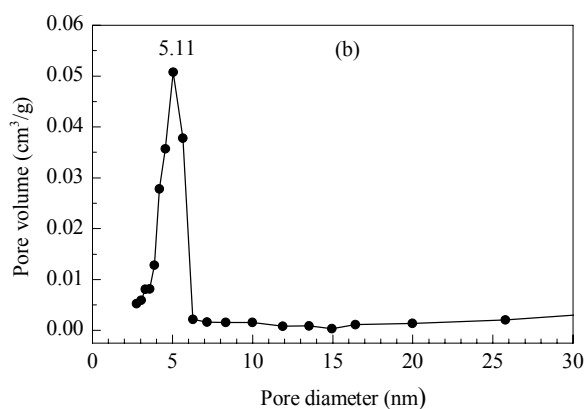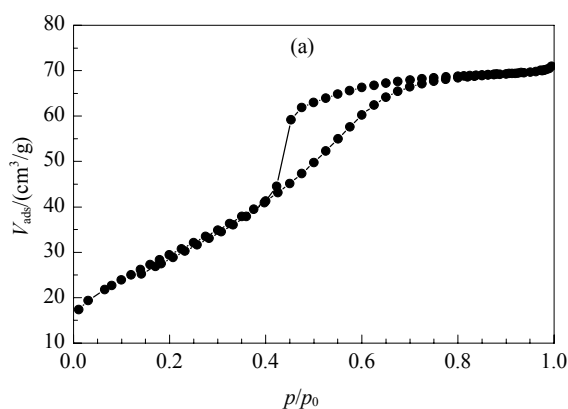 3(c), the lattice fringe measured in the HRTEM image had an average interplanar spacing of 0.35 nm, which is that of TiO_2 (d101) in the corresponding wide angle XRD pattern [22–24]. The pore size and grain size were, respectively, 5–7 nm and 12–14 nm, which were in good agreement with the N_2 adsorption and XRD results. The selected area electron diffraction (SAED) pattern of the sample (Fig. 3(d)) showed a sequence of diffraction rings consistent with those expected of anatase TiO_2 [11,25].

2.4 N_2 adsorption

Figure 4 shows the N_2 adsorption isotherm and pore size distribution curve of the sample prepared at the calcining temperature of 600/500 °C. The specific surface area calculated from the linear part of the adsorption isotherm was 110.8 m^2/g. The N_2 adsorption-desorption isotherm was Type IV with a H_2 hysteresis, which is typical of mesoporous materials [26,27]. The average mesopore size estimated using the Barrett-Joyner-Halenda (BJH) approach from the desorption branch was 5.11 nm (Fig. 4(b)), which was in agreement with the pore size estimated from TEM images (Fig. 3). From the crystallite size of the sample, the mesopores were probably formed by the agglomeration and connection of adjacent nanoparticles in the sample, which were seen in the TEM results (Figs. 3(a) and (b)).

Fig. 4. N_2 adsorption isotherm (a) and pore size distribution (b) for the sample prepared at the calcining temperature of 600/500 °C.

2.5   XPS analysis

Figure 5 shows the XPS spectra of the nitrogen doped mesoporous TiO_2 sample prepared with the calcining temperature of 600/500 °C and mole proportion of urea and tetrabutyl titanate of 2:1. Obvious peaks of titanium, oxygen, nitrogen, and carbon were detected in Fig. 5(a). The binding energies of Ti 2p, O 1s, N 1s, and C 1s were 458.5, 531, 400, and 284 eV, respectively, which was approximately in agreement with the data of other researchers [28–30]. The carbon signal was from the residual carbon from the precursor solution and adventitious hydrocarbon in the XPS instrument itself. The total nitrogen concentration, estimated from the XPS data, was 0.6% (molar ratio of elements).

Figure 5(b) shows the high resolution XPS spectra of the N 1s region. Three XPS peaks at 397.0, 398.8, and 402.4 eV were observed. Different N 1s peak positions represent various forms of nitrogen in doped TiO_2. In most cases, the peak at 397.0 eV was ascribed to the Ti–N–Ti bond indicating that nitrogen atom was substitutionally doped into the TiO_2 lattice [31–33]. The peak at 400 eV is related to oxidized nitrogen such as Ti–O–N or Ti–N–O bonding, so the peak at 398.8 eV can be attributed to anionic N^- in interstitial N [31,32,34]. The peak at 402.4 eV was observed and attrib-
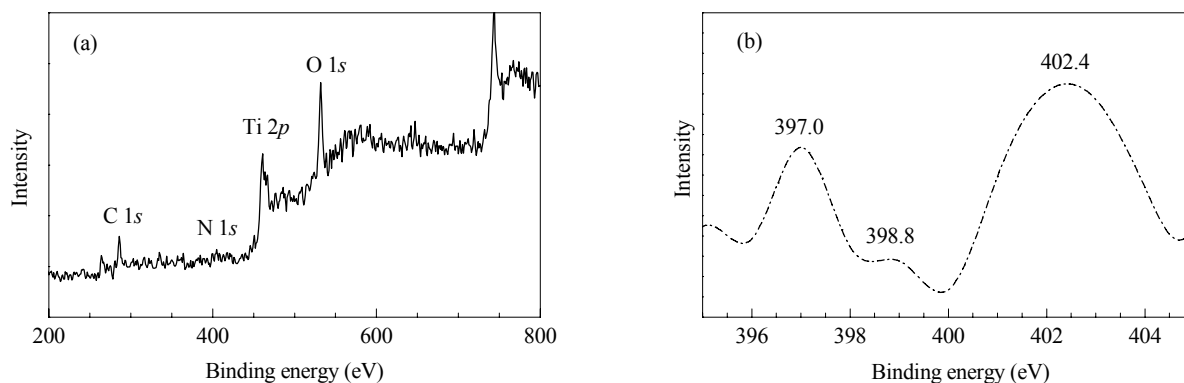
Fig. 5. XPS spectra (a) and high resolution XPS spectra of N 1s (b) for the nitrogen doped mesoporous TiO$_2$.

uted to molecularly chemisorbed γ-N$_2$, in which N atoms were incorporated into the TiO$_2$ lattice as N$_2$ molecules [12,35]. In Fig. 5(b), the peaks at 402.4 and 397.0 eV have a higher intensity than the peak at 398.8 eV. From the XPS results, it was concluded that the forms of doped nitrogen incorporated into the TiO$_2$ lattice were mainly substitutional N and molecularly chemisorbed γ-N$_2$ molecules, with some interstitial N. According to the literature [31,36,37], interstitial nitrogen doping is favored with oxygen-rich and low calcining temperature conditions, while substitutional nitrogen doping is preferred with the absence of oxygen and high calcining temperature conditions. In the present work, the first calcining was performed in N$_2$, which is an oxygen-deficient condition, and at a high calcining temperature (600 °C), so the nitrogen atoms were mainly incorporated into substitutional sites.

2.6 UV-Vis DRS spectra

Figure 6 shows the UV-Vis diffuse reflectance spectra of undoped and nitrogen doped mesoporous TiO$_2$ photocatalysts prepared with different mole ratios of urea and tetrabutyl titanate and at the calcining temperature of 600/500 °C. All the absorption band edges of the nitrogen doped mesoporous TiO$_2$ samples exhibited an evident red shift, and the light absorption intensity of the nitrogen doped samples was higher than that with undoped TiO$_2$ (S$_4$). As seen in Fig. 6(a), pure anatase TiO$_2$ showed absorption peaks at 400 nm. This may be because in the present work, the pure anatase TiO$_2$ was prepared in a N$_2$ atmosphere and high temperature and has oxygen vacancies, which contributed to the absorption red shift of oxygen-deficient TiO$_2$ [38]. With the increase of the mole ratio of urea and tetrabutyl titanate, the absorption intensity of visible light of the nitrogen doped samples increased. When the mole ratio of urea and tetrabutyl titanate was 2:1 (S$_1$), the absorption intensity of visible light was the highest. That is, absorption intensity increased with increasing nitrogen doping concentration. The light absorbance enhancement in the UV-visible light range was consistent with the yellow color of the sample. The enhanced light absorption in the visible range of the nitrogen doped samples was because nitrogen doping significantly shifted light absorption to the visible region through band gap narrowing [36–39].
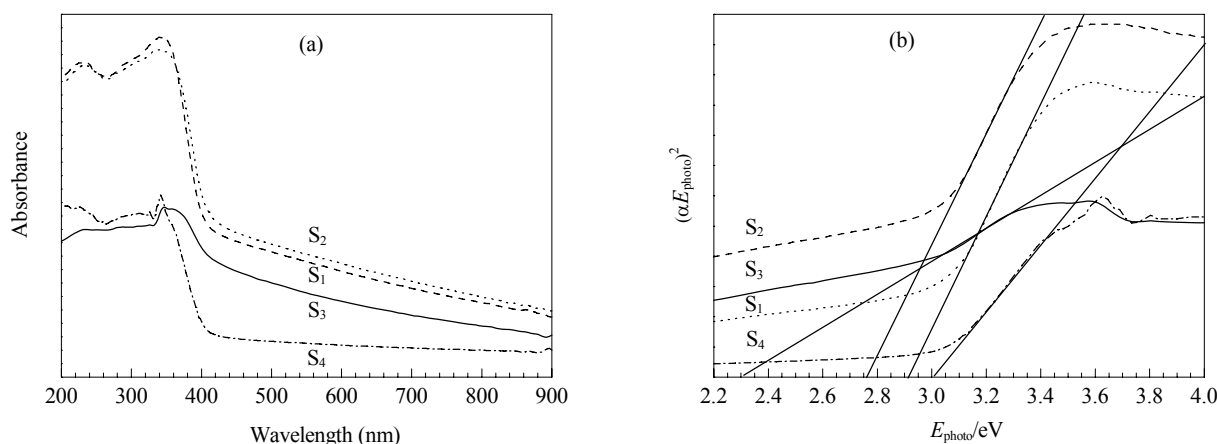

Fig. 6. UV-Vis DRS spectra (a) and band gap from the plots of (αE_{photon})^2 vs energy of absorbed light (b) of samples prepared with different mole ratios of urea and tetrabutyl titanate. S$_1$: CO(NH$_2$)$_2$:TiO$_2$ = 2:1; S$_2$: CO(NH$_2$)$_2$:TiO$_2$ = 1:1; S$_3$: CO(NH$_2$)$_2$:TiO$_2$ = 1:2; S$_4$: TiO$_2$.

Figure 6(b) shows the absorption edge of the samples. The plots of $(\alpha E_{photon})^2$ versus energy of absorbed light gave the band gap of the samples [32,40,41]. The band gap energies were measured to be 2.3–2.9 eV for the samples prepared with various mole proportion of urea and tetrabutyl titanate. The narrowed band gap was due to the contributions of the nitrogen dopant and oxygen vacancies in the TiO_2 lattice. The nitrogen dopant induced local states above the valence band edge and oxygen vacancies gave rise to mid-gap states below the conduction band [31,33,34,42]. These were responsible for the photocatalytic degradation reaction under visible light irradiation. S_3 has the lowest band gap energy, but its absorption intensity was also the lowest. So, taking into account band gap energy and absorption intensity, S_2 was the best sample.

2.7　Photocatalytic activity

The photocatalytic activity of the samples was measured by the degradation of MO solutions under visible light irradiation at room temperature. Figure 7 shows the degradation kinetics of the MO solutions. A blank test indicated that in the absence of a photocatalyst, decoloration of the MO solution was negligible. Compared with undoped mesoporous TiO_2, the nitrogen doped mesoporous TiO_2 photocatalysts showed obviously promoted photocatalytic activity. The degradation rates of all the nitrogen doped mesoporous TiO_2 photocatalysts were more than 60% for 12 h of irradiation time, while it was below 20% for undoped mesoporous TiO_2. The higher photocatalytic activity of the nitrogen doped TiO_2 photocatalysts under visible light irradiation was explained by the following. Nitrogen doping resulted in the shift of the absorbance of light towards longer wavelength. As shown in Fig. 6, the nitrogen doped mesoporous TiO_2 exhibited strong absorption in the visible light region,

while the undoped mesoporous TiO_2 absorbed only in the UV region. From Fig. 7, the photocatalytic activity sequence of the nitrogen doped mesoporous TiO_2 photocatalysts was $S_2 > S_3 > S_1$. The sequence of the mole ratios of urea and tetrabutyl titanate of the three samples was $S_1 > S_2 > S_3$. This result indicated that with an appropriate amount of nitrogen doping, photoexcited electrons and holes can be separated efficiently and the photocatalytic activity was enhanced, but excessive nitrogen doping may act as the recombination centers for photoexcited electrons and holes, which reduces the photocatalytic activity [43]. The photocatalytic activity of the nitrogen doped mesoporous TiO_2 samples was in agreement with their UV-Vis diffuse reflectance spectra.

3　Conclusions

Nitrogen doped mesoporous TiO_2 with high crystallinity and a large specific surface area was fabricated using a sol-gel method in which PAM and PEG were used as templates. When calcined in N_2, PAM was converted into a sturdy, and the amorphous carbon that prevented the collapse of the mesoporous structure when the sample was calcined to the temperature required for getting high crystallinity. When the mass ratio of PAM and PEG was 1:4, the sample prepared at 600 °C in nitrogen and at 500 °C in air has the anatase phase, and it has a mesoporous structure with high crystallinity and a high specific surface area. The absorption band edges of the nitrogen doped mesoporous TiO_2 samples exhibited a red shift and their absorption intensity was higher than that of the undoped sample, that is, nitrogen doping made the band gap of TiO_2 narrower. Compared with the undoped sample, nitrogen doped mesoporous TiO_2 has a higher photocatalytic activity under irradiation of visible light.
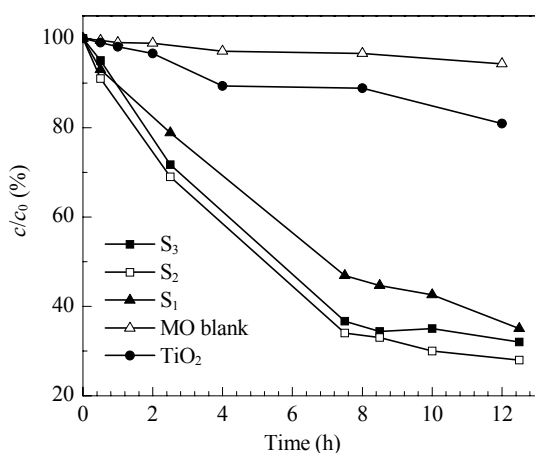

Fig. 7. Photocatalytic degradation kinetics of MO solutions under visible light irradiation.

References

1　Wu C W, Ohsuna T, Kuwabara M, Kuroda K. *J Am Chem Soc*, 2006, **128**: 4544

2　Wan Y, Yang H F, Zhao D Y. *Acc Chem Res*, 2006, **39**: 423

3　Hao H Y, Zhang J L. *Microporous Mesoporous Mater*, 2009, **121**: 52

4　向全军, 余家国. 催化学报 (Xiang Q J, Yu J G. *Chin J Catal*), 2011, **32**: 525

5　Bleta B, Alphonse P, Lorenzato L. *J Phys Chem C*, 2010, **114**: 2039

6　Liu Y J, Szeifert J M, Feck J M, Mandmeier B, Rathousky J, Hayden O, Fattakhova-Rohlfing P, Bein T. *ACS Nano*, 2010, **4**: 5373

7　Liu S W, Yu J G, Jaroniec M. *Chem Mater*, 2011, **23**: 4085

8　Kim D S, Kwak S Y. *Appl Catal A*, 2007, **323**: 110

9　Serrano D P, Calleja G, Sanz R, Pizarro P. *J Mater Chem*, 2007, **17**: 1178

10　Liang G, Xu J, Xu W, Shen X, Zhang H, Yao M. *J Optoelectron Adv Mater*, 2010, **12**: 1758

11　Lee J, Oriall M C, Warren S C, Kamperman M, Disalvo F J, Wiesner U. *Nature Mater*, 2008, **7**: 222

12　Asahi R, Morikawa T, Ohwaki T, Aoki K, Taga Y. *Science*, 2001, **293**: 269

13　Liu G, Yang H G, Wang X W, Cheng L N, Pan J, Lu G Q, Cheng H M. *J Am Chem Soc*, 2009, **131**: 12868

14　Cong Y, Zhang J L, Chen F, Anpo M, He D N. *J Phys Chem C*, 2007, **111**: 10618

15　Yang K S, Dai Y, Huang B B, Whangbo M H. *J Phys Chem C*, 2009, **113**: 2624

16　Pan J H, Zhang X W, Du A J, Sun D D, Leckie J O. *J Am Chem Soc*, 2008, **130**: 11256

17　Liu S W, Yu J G, Cheng B, Jaroniec M. *Adv Colloid Interface Sci*, 2012, **173**: 35

18　Periyat P, Mccormack D E, Hinder S J, Pillai S C. *J Phys Chem C*, 2009, **113**: 3246

19　Xu P, Lu J, Xu T, Gao S M, Huang B B, Dai Y. *J Phys Chem C*, 2010, **114**: 9510

20　Wang D H, Jia L, Wu X L, Lu L Q, Xu A W. *Nanoscale*, 2012, **4**: 576

21　Tian G H, Fu H G, Jing L Q, Xin B F, Pan K. *J Phys Chem C*, 2008, **112**: 3083

22　Ren W J, Ai Z H, Jia F L, Zhang L Z, Fan X X, Zou Z G. *Appl Catal B*, 2007, **69**: 138

23　Zhang Y, Li J, Wang J. *Chem Mater*, 2006, **18**: 2917

24　Xu X M, Li X N, Lin P Y, Chen T, Yuan R S, Ding Z X, Wu L, Wang X X, Li Z H. *Chem Commun*, 2011, **47**: 2538

25　Wang D H, Ma Z, Dai S, Liu J, Nie Z M, Engelhard M H, Huo Q S, Wang C M, Kou R. *J Phys Chem C*, 2008, **112**: 13499

26　Yu J C, Zhang L Z, Yu J G. *Chem Mater*, 2002, **14**: 4647

27　Wang X J, Hu D D, Yang J X. *Chem Mater*, 2007, **19**: 2610

28　Irie H, Watanabe Y, Hashimoto K. *J Phys Chem B*, 2003, **107**: 5483

29　Choi H, Antoniou M G, Pelaez M, Dela Cruz A A, Shoemaker J A, Dionysiou D D. *Environ Sci Technol*, 2007, **41**: 7530

30　Shieh D L, Lin Y S, Yeh J H, Chen S C, Lin B C, Lin J L. *Chem Commun*, 2012, **48**: 2528

31　Wang J, Tafen D N, Lewis J P, Hong Z L, Manivannan A, Zhi M J, Wu N Q. *J Am Chem Soc*, 2009, **131**: 12290

32　Mitoraj D, Kisch H. *Angew Chem, Int Ed*, 2008, **47**: 9975

33　Etacheri V, Seery M K, Hinder S J, Pillai. *Chem Mater*, 2010, **22**: 3843

34　Yang G D, Jiang Z, Shi H H, Xiao T C, Yan Z F. *J Mater Chem*, 2010, **20**: 5301

35　Morikawa T, Asahi R, Ohwaki T, Aoki K, Taga Y. *Jpn J Appl Phys*, 2001, **40**: 561

36　Xiang Q J, Yu J G, Jaroniec M. *Phys Chem Chem Phys*, 2011, **13**: 4853

37　Xiang Q J, Yu J G, Wang W G, Jaroniec M. *Chem Commun*, 2011, **47**: 6906

38　Lin Z, Orlov A, Lambert R M, Payne M C. *J Phys Chem B*, 2005, **109**: 20948

39　Spadavecchia, F, Cappelletti G, Ardizzone S, Bianchi C L, Cappelli S, Oliva C, Scardi P, Leoni M, Fermo P. *Appl Catal B*, 2010, **96**: 314

40　Wu G S, Nishikawa T, Ohtani B, Chen A C. *Chem Mater*, 2007, **19**: 4530

41　Zabek P, Eberl J, Kisch H. *Photochem Photobiol Sci*, 2009, **8**: 264

42　Fujishima A, Zhang X T, Tryk D A. *Surface Science Reports*, 2008, **63**: 515

43　张晓茹, 林艳红, 张健夫, 何冬青, 王德军. 物理化学学报 (Zhang X R, Lin Y H, Zhang J F, He D Q, Wang D J. *Acta Phys-Chim Sin*), 2010, **26**: 2733